Validation of Chemically Reactive Computational Fluid Dynamics Simulations of Oblique Detonation Wave Engines

Alexander Marshak¹ and Ralf Deiterding²

Department of Aeronautics and Astronautics, University of Southampton, Boldrewood Innovation Campus, Southampton, SO16 7QF, United Kingdom

In this study, external injection oblique detonation wave engine (ODWE) experiments are simulated using AMROC (Adaptive Mesh Refinement in Object-oriented C++), our block-structured, adaptive mesh refinement framework for the simulation of shock-induced combustion phenomena. Simulations in the midplane of the experimental combustion system are conducted using a two-dimensional domain with accurate embedded boundaries to create the geometry of the inlet ramp, combustor, and nozzle. The external injection system and mixing process are simplified to a perfectly mixed fuel-air stream with a known freestream Mach number, temperature, and pressure. Comparisons between numerical and experimental results are made using measured combustor wall pressures, oblique shockwave (OSW) angles, and detonation wave angles. Here, we provide all setup details that have allowed us to achieve full CFD validation for three prototype ODWE configurations experimentally investigated by Zhang et al. at the Chinese Academy of Sciences. The successful application of simple, perfectly premixed inflow conditions makes these configurations now easily accessible and provides a set of fully reproducible ODWE benchmarks for other high-speed combustion codes.

I. Nomenclature

 L_c = combustion chamber length L_w = detonation front length M_{∞} = freestream Mach number $P_{s,\infty}$ = freestream static pressure R_m = specific gas constant of mixture $T_{s,\infty}$ = freestream static temperature β_s = oblique shockwave angle β_w = oblique detonation wave angle Φ = equivalence ratio

II. Introduction

To extend the envelope of airbreathing hypersonic flight above Mach 10, it is proposed that an ODWE, also known as a shock-induced combustion ramjet (shcramjet), will have a meaningful performance advantage over scramjets and increase the maximum operational velocity. Unlike the diffusive mixing and burning process used inside a scramjet combustor, an ODWE operates using an oblique detonation wave (ODW). This phenomenon occurs when a fuel-air mixture travelling at hypersonic speed impinges on a wedge. This creates an oblique shockwave, raising the pressure and temperature until ignition conditions are met, and a chemical reaction occurs downstream of the wedge front,

¹ Undergraduate Student. (am6g21@soton.ac.uk)

² Professor of Numerical Methods in Fluid Dynamics, Senior Member. (r.deiterding@soton.ac.uk)

increasing the pressure and temperature of the flow. The exhaust then expands to create thrust in the same way as a scramjet. The ODWE cycle can be expressed as:

Compression + Fuel addition (Mixing) \rightarrow (Compression + Burning) \rightarrow Expansion

Using shock-induced combustion, the combustor length of an ODWE can be significantly shorter than a scramjet, reducing vehicle size and engine weight.

For most analyses of ODWEs and the experiment studied in this report, hydrogen is used as fuel, as it has the highest lower calorific value of any common fuel. Additionally, mixing is faster than alkanes and other hydrocarbons, allowing for a shorter mixing duration, reducing the length of the vehicle.

Two methods of introducing a fuel-air mixture into the combustor can be used: external or internal fuel injection. Figure 1 shows the configuration of an external injection ODWE, where fuel is injected on the forebody of the vehicle. The mixing process starts at the compression ramp, removing the need for a mixing duct and reducing the length and weight of the engine.

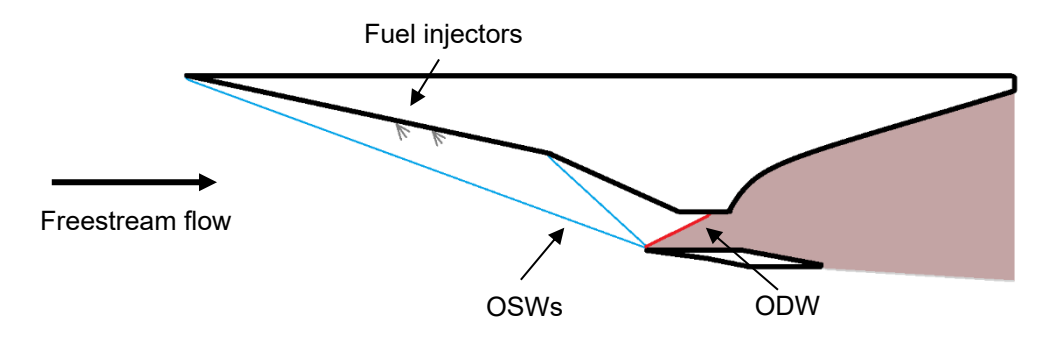


Fig. 1 Diagram of a two-stage external injection ODWE.

To date, only a very small number of ODWE experiments have been performed, due to the complex and expensive setups of large hypersonic wind tunnels. Therefore, the use of computational fluid dynamics (CFD) simulations is necessary for the analysis of ODWE combustors and inlet geometries. For this reason, validation of CFD methods using present experimental setups is essential for further experiments and simulations of ODWEs.

Our analysis focuses on external injection ODWE experiments performed by Zhang et al. [1] at the Chinese Academy of Sciences. The method used in this report differs notably from their two-step CFD approach [2]. Here, we simulate the full configuration in a single computation, including the inlet ramp, which reduces the overall computational costs on the one hand, but also allows investigation of interaction effects between inlet ramp and combustor entry on the other. The simulations in this study use AMROC (Adaptive Mesh Refinement in Object-oriented C++) [3], our block-structured, adaptive mesh refinement framework for the simulation of shock-induced combustion phenomena. The method uses immersed boundary conditions on a Cartesian mesh that is dynamically adapted to embedded geometries and flow features by applying regular refinement patches [4].

III. Governing Equations and Numerical Methods

The investigations in this report focus on viscous two-dimensional chemically reactive CFD simulations using H_2 – air mixtures. For the purposes of accurate initiation time measurements and modelling of boundary layers on external injection ODWEs, viscous effects must be considered.

A. Governing Equations

The multi-species Navier-Stokes equations with a detailed chemical model in three-dimensional form are solved as governing equations:

$$\frac{\partial Q}{\partial t} + \frac{\partial (F - F_{V})}{\partial x} + \frac{\partial (G - G_{V})}{\partial y} = S, \qquad (1)$$

where $Q = [\rho_i \quad \rho u \quad \rho v \quad \rho E]^T$ are the conservative variables and $F = [\rho_i u \quad \rho u^2 + p \quad \rho uv \quad (\rho E + p)u]^T$ and $G = [\rho_i v \quad \rho uv \quad \rho v^2 + p \quad (\rho E + p)v]^T$ are the convective in the *x*- and *y*-direction, respectively. $S = [\dot{\omega}_i \quad 0 \quad 0 \quad 0]^T$ are chemical source terms, where $i = 1, 2, ..., N_{\rm sp}$. $N_{\rm sp}$ is the total number of species and ρ_i is the density of component *i*. The multi-species ideal gas state equation reads

$$p = \sum_{i=1}^{N_{\infty}} \rho_i \frac{R_{\rm u}}{W_i} T . \tag{2}$$

E denotes the total unit energy and is given as

$$E = \sum_{i=1}^{N_{sp}} Y_i h_i - \frac{p}{\rho} + \frac{1}{2} (u^2 + v^2),$$
(3)

where h_i is the specific enthalpy of species i computed by

$$h_{i} = h_{\text{ref},i}^{0} + \int_{T_{-s}}^{T} c_{p_{i}} dT.$$
 (4)

The specific heat at constant pressure c_{p_i} of species *i* depends on the temperature and is calculated by a polynomial of degree 4 by the Chemkin II library [5]. The viscous fluxes are given as

$$F_{V} = \begin{bmatrix} J_{x,i} & & & \\ \tau_{xx} & & & \\ \tau_{xy} & & & \\ k\frac{\partial T}{\partial x} + \sum_{j=1}^{N_{xy}} h_{j}J_{x} + u\tau_{xx} + v\tau_{xy} \end{bmatrix}, G_{V} = \begin{bmatrix} J_{y,i} & & & \\ \tau_{yx} & & & \\ \tau_{yy} & & & \\ k\frac{\partial T}{\partial y} + \sum_{j=1}^{N_{xy}} h_{j}J_{y} + u\tau_{xy} + v\tau_{yy} \end{bmatrix}, \tag{5}$$

where the diffusion fluxes $J_{x,i}$, $J_{y,i}$ are related to the species gradients by Fick's law:

$$J_{i} = \rho Y_{i} \left[\left(-\frac{1}{X_{i}} \right) D_{i} \left(\nabla X_{i} + (X_{i} - Y_{i}) \frac{\nabla P}{P} \right) - \frac{D_{i}^{T}}{\rho Y_{i}} \frac{\nabla T}{T} \right], \tag{6}$$

with D_i^T denoting the mixture-averaged thermal diffusion coefficient, which are calculated through the Chemkin II Transport library [5]. In the momentum and energy fluxes, τ denotes the viscous stresses. The stresses in all directions are evaluated as

$$\tau_{xx} = -\frac{2}{3}\mu(\nabla \cdot \mathbf{v}) + 2\mu \frac{\partial u}{\partial x}, \ \tau_{xy} = \tau_{yx} = \mu \left(\frac{\partial u}{\partial y} + \frac{\partial v}{\partial x}\right), \ \tau_{yy} = -\frac{2}{3}\mu(\nabla \cdot \mathbf{v}) + 2\mu \frac{\partial v}{\partial y}, \nabla \cdot \mathbf{v} = \left(\frac{\partial u}{\partial x} + \frac{\partial v}{\partial y}\right). \tag{7}$$

 $\dot{\omega}_i$ is the mass generation rate of component i, which is calculated by a chemical reaction mechanism of J steps as

$$\dot{\omega}_{i} = \sum_{j=1}^{J} \left(v_{ji}^{r} - v_{ji}^{f} \right) \left[k_{j}^{f} \prod_{n=1}^{N_{sp}} \left(\frac{\rho_{n}}{W_{n}} \right)^{v_{jn}^{f}} - k_{j}^{r} \prod_{n=1}^{N_{sp}} \left(\frac{\rho_{n}}{W_{n}} \right)^{v_{jn}^{r}} \right], \quad i = 1, \dots N_{sp}.$$
 (8)

The rate constants of forward and reverse chemical reactions are given by the Arrhenius formula:

$$k_j^{\text{f/r}}(T) = A_j^{\text{f/r}} T^{\beta_j^{\text{f/r}}} \exp\left(-\frac{E_j^{\text{f/r}}}{RT}\right). \tag{9}$$

Two chemical reaction models are used in AMROC simulations in this report: the hydrogen-oxygen mechanism from the larger hydrocarbon mechanism developed by C. Westbrook [6], and the hydrogen-air mechanism from C. Jachimowski [7]. In total, the Westbrook mechanism consists of 34 elementary reactions among 8 species (H_2 , H, O_2 , O, OH, HO_2 , H_2O_2 , H_2O) with N_2 and Ar added as inert species. The Jachimowski mechanism has 19 elementary reactions among the same reactive species.

B. Numerical Methods

A hybrid Roe-HLL (Harten–Lax–van Leer) Riemann solver with dimensional splitting is utilized to discretize the upwind fluxes F and G, and the MUSCL-TVD scheme with Minmod limiter is employed for the reconstruction. The diffusion terms in F_v and G_v are discretized by a central difference scheme formulated in conservative flux form. A semi-implicit generalized Runge-Kutta scheme is adopted for the integration of the chemical kinetics $\dot{\omega}_i$ [8] and a dynamic time step is utilized with a CFL of 0.9. A level-set approach with the ghost fluid method [4] is employed to represent the embedded solid wall boundaries. While the Cartesian scheme is second order accurate throughout, the spatial order drops to one at the embedded boundary.

The numerical scheme is used within the block-structed adaptive mesh refinement algorithm (AMR), originally developed by Berger and Colella [9]. In this approach, refinement grids are created recursively from coarser ones, using a specific refinement factor for each level, with a hierarchy of successively embedded levels constructed, and hierarchically refined time steps being applied. The mesh adaptivity permits regions of high fluid field complexity to be flagged and discretized into smaller volume cells, efficiently refining the grid only where it is necessary. The AMR method is implemented in our generic, dimension independent object-oriented framework in C++, known as AMROC [10]. A parallelization strategy based on rigorous domain decomposition is used, allowing simulations to be run on multiple nodes on Iridis 5, the University of Southampton's high performance computing system.

Prior to this project, the AMROC combustion solver has been comprehensively validated for many different high-speed combustion scenarios, including detonation propagation [11], detonation-boundary layer interaction [12], flame acceleration and detonation-to-deflagration transition [13], and auto-ignition [14].

IV. Reported Experimental Conditions

Figure 2 shows the geometry of the large-scale ODWE test apparatus inside the JF-12 wind tunnel, at the Institute of Mechanics, Chinese Academy of Sciences, arranged by Zhang et al [1]. The model consists of a 15° inclined inlet ramp with external hydrogen injectors, followed by a combustor and nozzle angled down at 15° to achieve a total flow deflection of 30° at the combustor inlet. Hydrogen gas is injected into the core airflow through sonic transverse jets upstream of the OSW before entering the combustor, where a standing ODW forms. The combustor is in the shape of a rectangular channel, which is 0.0765 m in height and 0.4 m in width. The length of the upper wall of the combustor (L_c) is adjustable by moving it upstream, while the lower wall is at a fixed length of 0.2 m. Downstream of the combustor, a simple angled nozzle is installed, with a length of 0.4 m, which diverges at 15°. Measurement methodologies include high-speed schlieren photography, and an arrangement of pressure transducers and thermocouples along the midplane. Two tests were conducted, one with a shorter L_c , designed to produce a strong ODW, and the other with a longer L_c to produce a weak (shallow) ODW. The reported test conditions of each run are listed in Table 1.

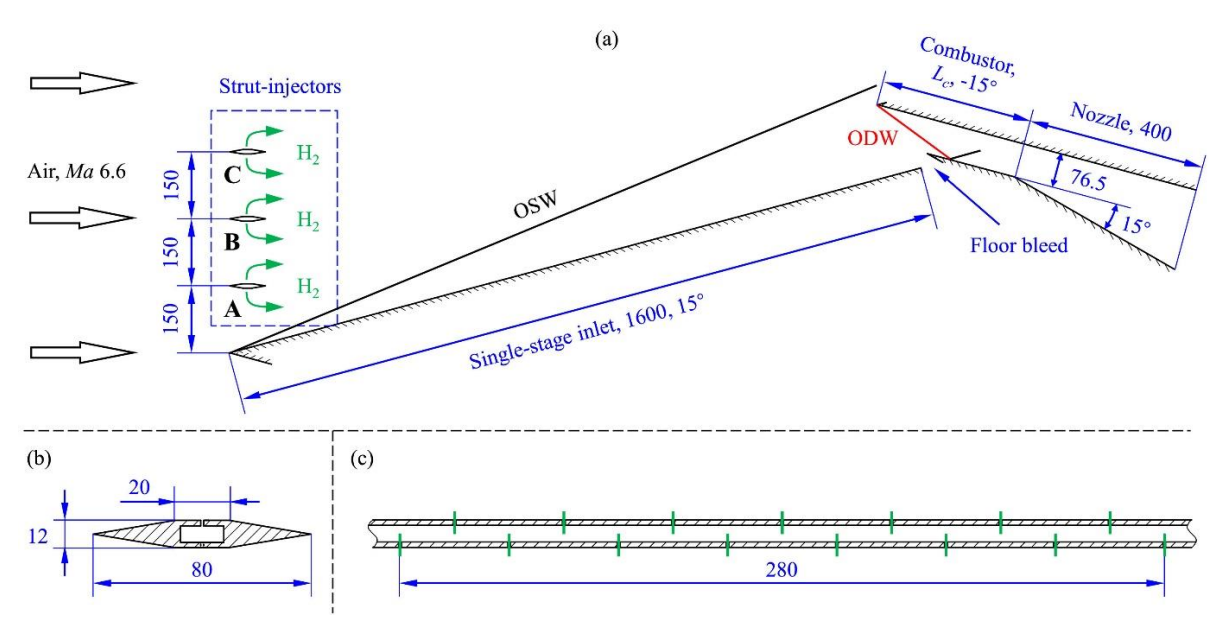


Fig. 2 Geometry of ODE model (dimensions in mm): a) global side view, b) cross section of one strut injector, and c) front view of strut injector.

In addition to these experiments, a further investigation was made with the same ODWE model using laser absorption spectroscopy (LAS) [15] to confirm that detonative combustion was occurring. This was achieved using the short combustor wall to produce a strong ODW, which is used here as a second experiment for validation. In addition to OH partial pressure measurements, schlieren images of the start-up sequence were included, and shock positions were measured throughout the run. The reported test conditions are listed below in Table 2.

Table 1 Reported test conditions and strut injector arrangement.

Test No.	20190705	20190710
ODW Type	Strong	Weak
Freestream stagnation temperature [K]	3525	3377
Freestream stagnation pressure [kPa]	2450	2260
Freestream Mach number	6.6	6.6
Combustor length L_c [m]	0.26	0.41
Strut injectors used	A	A, B
Hydrogen mass flow rate [gs ⁻¹]	19.6	36.7

Table 2 Reported test conditions for LAS experiment.

Test Name	Run 1 (Schlieren)
ODW Type	Strong
Combustor length L_c [m]	0.26
Freestream stagnation temperature [K]	3852
Freestream stagnation pressure [kPa]	2540
Freestream Mach number	6.47
Freestream static temperature [K]	491
Freestream static pressure [kPa]	0.551
Freestream velocity [ms-1]	2876
Hydrogen injection pressure [kPa]	2740
Hydrogen mass flow rate [gs ⁻¹]	19.8

IV. Estimation of Inflow Conditions

The reported test conditions do not provide sufficient information to determine the necessary freestream conditions for a mixed fuel-air stream. The equivalence ratio at the midplane of the combustor inlet must be determined, along with the specific gas constant of the freestream flow to calculate the freestream Mach number. Since freestream static pressures and temperatures were not reported, these were interpolated from inflow conditions described in other experiments using the JF-12 tunnel [15, 16, 17].

The stoichiometry of the mixture after hydrogen injection has a large impact on the Mach number at the combustor inlet. For a constant freestream Mach number, a greater equivalence ratio corresponds to a decreasing post-mixed Mach number, due to the increasing specific gas constant of the mixture (R_m) . The velocity of the post-mixed gas is calculated using conservation of momentum, since the injected hydrogen is significantly slower than the freestream air. Using the mass fractions of the gas mixture, the average molar mass, specific gas constant, specific heat ratio and specific heat capacity of the mixture were calculated. Specific heat capacities for each species are obtained from The

Engineering Toolbox database [18]. From these, the freestream Mach number can be calculated for a given equivalence ratio.

Several parameter studies were conducted to refine the equivalence ratio for the strong and weak cases. 3D simulations of the hydrogen injectors and inlet ramp [2] predict an equivalence ratio of 0.35 at the combustor inlet for the strong ODW case, which was used as a starting point for numerical simulations.

V. Freestream Parameters and Geometry

Using the specified inlet ramp and combustor geometries, artificial embedded boundaries were added to the simulation domain to create a 2D section of the ODWE. The vertices defining the boundaries for the strong and weak cases and the full numerical setup for each case can be found in Sections A and B of the appendix. In Table 3, we report the detailed inflow parameters which allowed us to achieve CFD validation with our 2D midplane simulations for the experiments by Zhang et al.

Case Type	Strong	Weak	LAS
M_{∞}	6.037	4.60	5.912
$P_{s,\infty}$ [kPa]	0.332	0.550	0.355
$T_{s,\infty}$ [K]	429.9	410.3	491
Φ	0.460	0.820	0.465

Table 3 Freestream parameters for numerical simulation

VI. Results for Strong Case

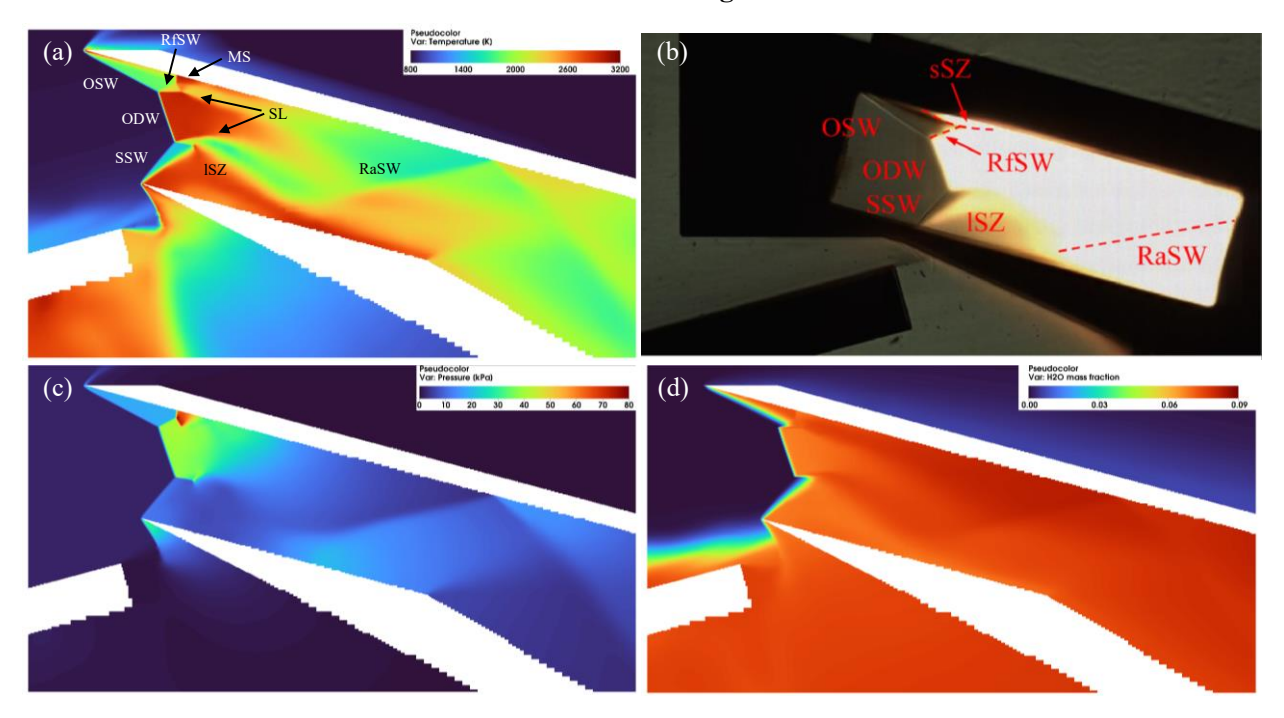


Fig. 3 Numerical flow field within combustor for strong case: (a) temperature, (b) experiment schlieren image, (c) pressure, (d) H₂O mass fraction.

In Fig. 3, the numerical flow field of our simulation, using the Westbrook mechanism, is compared with the schlieren photography from the experiment report. The full numerical domain of the strong case, including the inlet ramp geometry, is provided in Section C of the appendix. An OSW is formed at the inlet ramp, which extends above

the upper combustor wall, and provides steady flow to the combustor. From Fig. 3(a) and 3(b), the strong ODW case is shown to be modelled accurately, with the OSW, ODW, secondary shockwave (SSW), reflected shockwave (RfSW), lower separation zone (LSZ) and reattachment shockwave (RaSW) resolved. Two slip lines (SL) are formed as the flow is decelerated considerably further through the ODW than the surrounding regions. The detonation front length (L_w) of 37 mm, measured in the experiment, closely agrees with our simulation, at 35mm, while the observed ODW angle (β_w) of 83.8° is slightly shallower than seen in the simulation (86.3°). Our reported post-detonation conditions are 39 kPa and 2900 K, averaged across the ODW.

Instead of a separation zone (sSZ) reported in the experiment, the simulation predicts a Mach reflection (MR), where the RfSW is the incident shockwave which is attached to a Mach stem (MS). This creates a large pressure spike at 6.75 cm from the leading edge of the upper wall, shown in Fig. 4(a). Greater numbers of pressure transducers in this region would be necessary to confirm whether MR is present in the experiment, or whether a shockwave-boundary layer interaction takes place.

The H₂O distribution, plotted in Fig. 3(d), demonstrates the need for the bleed duct, as a reacting boundary layer forms on the inlet ramp which is successfully bled away from the combustor. At the OSW, decoupled shock-induced combustion (DSIC) occurs, as the induction region spans 6.5 mm behind the leading shockwave. At the lip of the lower wall, a rarefaction wave is present, with a considerably longer induction length of 9 mm due to the lower post-shock temperature. This is confirmed by the experiment image, which shows a dark region separating the SSW and the LSZ.

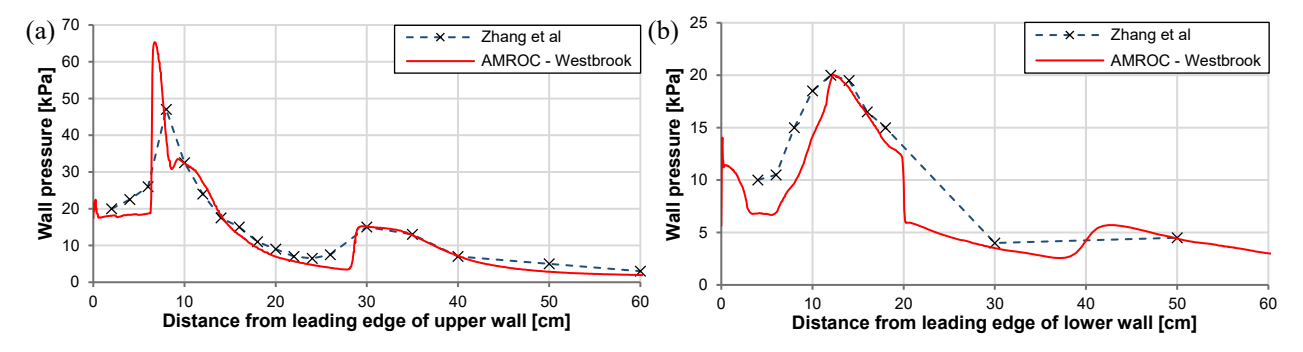


Fig. 4 Surface pressure distribution at combustor wall: (a) upper wall, (b) lower wall.

Pressure distributions of the combustor walls, presented in Fig. 4, show good agreement with experimental results. The large pressure peak at 6.75 cm is caused by the MS, and the RaSW is shown to intersect the upper wall in the correct location, as a secondary pressure peak is observed at 30cm from the leading edge in both the simulation and the experiment. At the lower wall, a large pressure peak is seen at 12.5 cm which is formed from the reattachment of the flow after the LSZ, creating a shockwave. The peak pressure of 20 kPa on the lower wall is matched by the experiment and confirms the correct freestream static pressure was used.

This simulation was achieved using a total of four refinement levels, so that sufficient resolution covered the induction zone of the ODW. The refinement factor between levels is always two. Scaled gradient criteria in overall density and static pressure are used to detect and refine flow features at runtime. The quasi-steady adapted mesh around the combustor is shown in Fig. 5. To obtain accurate flow fields, we required minimum cell dimensions of 0.65 mm x 0.37 mm. From these results, it can be demonstrated that the AMROC solver is capable of accurately simulating this complex flow field and has been validated for this case. Approximate CPU times on the Iridis-5 compute cluster, consisting of 40-core nodes with 2.0 GHz Intel Xeon processors, and total time steps are listed in Table 4.

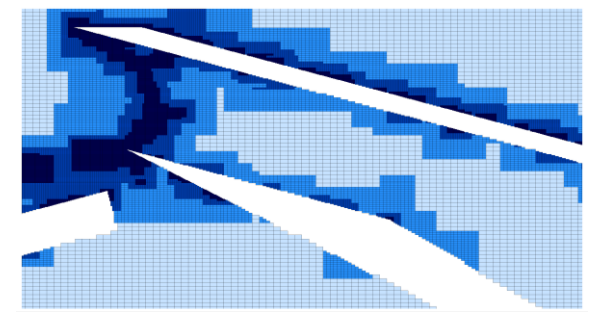


Fig. 5 Mesh refinement levels in simulation.

Table 4 Simulation time summary

Case Type	Strong	Weak	LAS
CPU time [hrs]	9611	2943	11705
Time steps	237,312	101,800	202,440

VII. Results for Weak Case

A. High Resolution Simulation

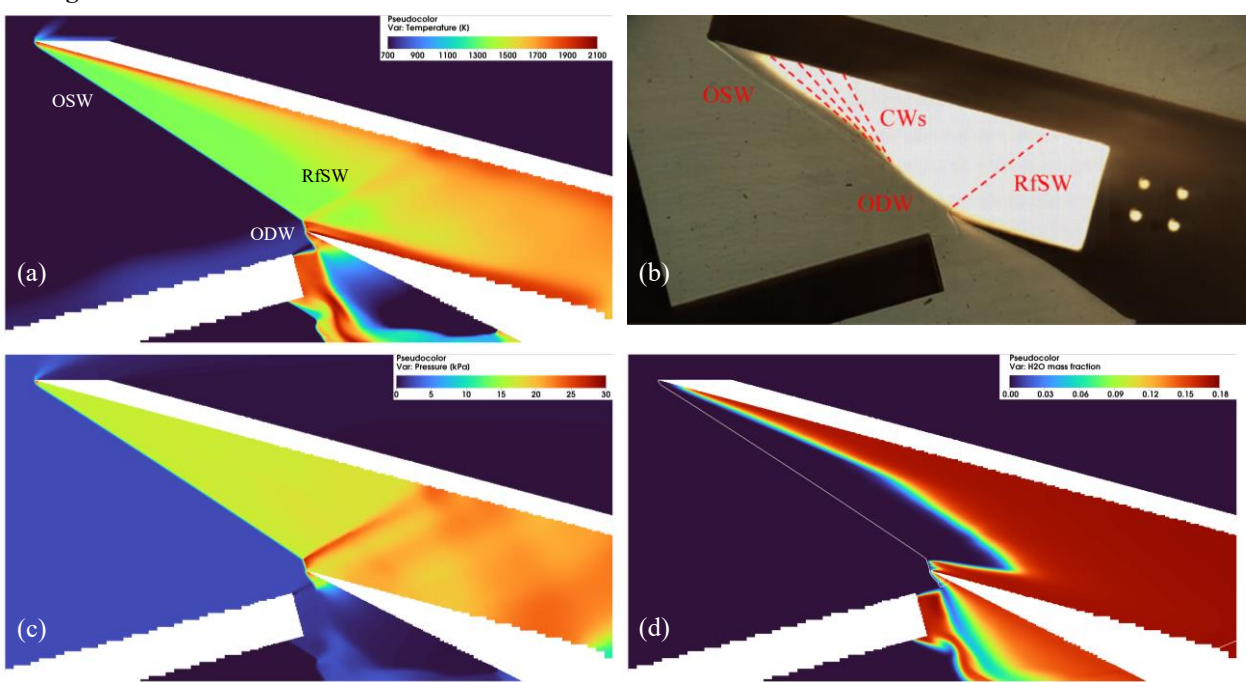


Fig. 6 Numerical flow field within combustor for weak case: (a) temperature, (b) experiment schlieren image, (c) pressure, (d) H₂O mass fraction with pressure contour.

Figure 6 presents the comparison between the experiment schlieren photography and the numerical flow field, achieved using the Jachimowski mechanism. The longer combustor inlet allows the leading OSW to reach the lower wall, where an ODW is formed. A RfSW is formed at the lip of the combustor, which forms a shock-train downstream, and is responsible for the multiple pressure peaks on the upper wall. The OSW angle (β_s) of 47.8° matches with our simulation ($\beta_s = 48.1$ °) and the shock front is loosely coupled to the flame front with a large induction zone, shown in Fig. 6(d), which is also seen in the schlieren image.

However, the ODW formation is much more pronounced in the experiment, and it is possible that there is some disturbance to the flow entering the combustor, either caused by a reactive boundary layer, or from boundary layer interactions at the upper wall, as the simulations predict deflagrative decoupled shock-induced combustion across the entire shock front. This inflow disturbance may have the effect of slowing and compressing the oncoming flow near the inlet ramp and thereby decreasing induction length. This causes the angle of the OSW to rise, increasing the coupling between the shock and flame front. Since the RfSW is at a greater angle relative to the oncoming flow in the experiment, the Mach number in this region of the combustor is likely to be lower than the simulated case.

B. Study of Boundary Layer Effects from Inlet Ramp

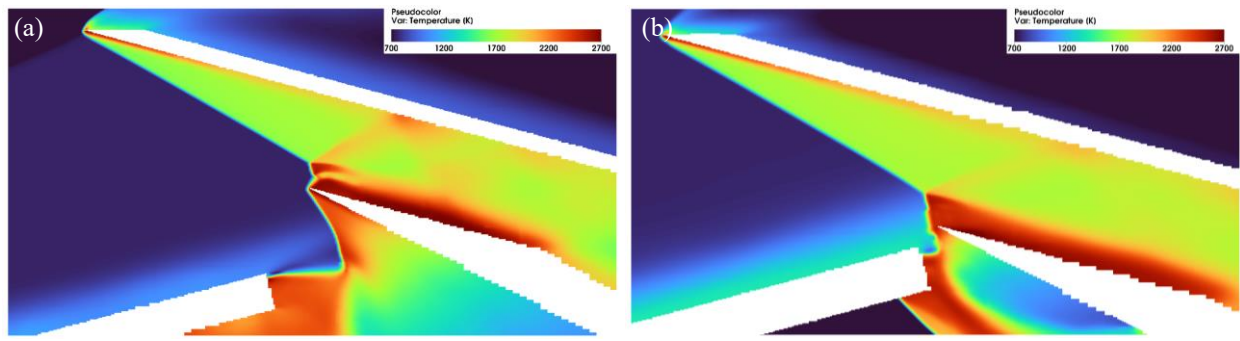


Fig. 7 Temperature plots for weak ODW: (a) no boundary layer, (b) full boundary layer.

Further studies of the weak ODW configuration were carried out to understand the effects of boundary layer formation along the inlet ramp on the exhibited shockwave structure. The ability to simulate the ramp and combustor in one simulation provides a means to study this effect in detail and can help explain the schlieren images presented in the experiment report. Two simulations were performed with an increased freestream Mach number of 5.5 to increase the temperature across the inlet ramp. In one simulation, the inlet ramp was translated downwards by 5 cm from the original geometry with the inflow conditions set to prevent boundary layer formation. In the second simulation, the original geometry is used, and a full reactive boundary layer is present. These simulations were carried out using three levels of mesh refinement, and both used the Jachimowski reaction mechanism.

Without the presence of a boundary layer, seen in Fig. 7(a), a strong ODW forms above the lower lip of the combustor, with the same structure discussed in Section VI. A rarefaction wave is present, and a separation zone forms at the lower wall, which is not seen in the experiment.

However, when a reactive boundary layer is present, shown in Fig. 7(b), the detonation front length is doubled, and the flow remains attached to the lower lip of the combustor. In this region, the induction length is 4.5 mm, and the shock and flame front are closely coupled. Compared to the reference case, when this large ODW is formed, the reflection point of the OSW is moved further upstream, which moves the reflection point of the RfSW forwards. In Fig. 8, this reflection point corresponds to the first pressure peak at 12 cm along the wall. While the smooth transition of OSW to ODW is not seen in this simulation, it is evident that some disturbance to the inlet flow in the experiment was likely present which would trigger a transition to ODW.

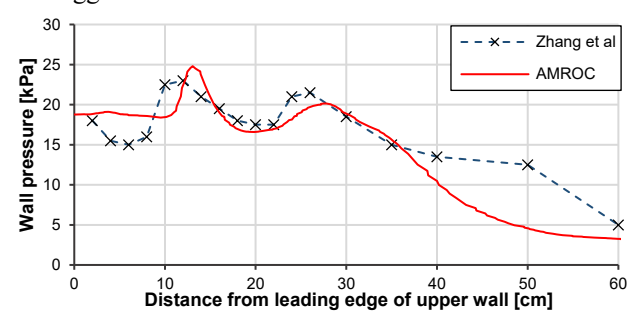


Fig. 8 Pressure distribution across upper wall.

VIII. LAS Strong Case

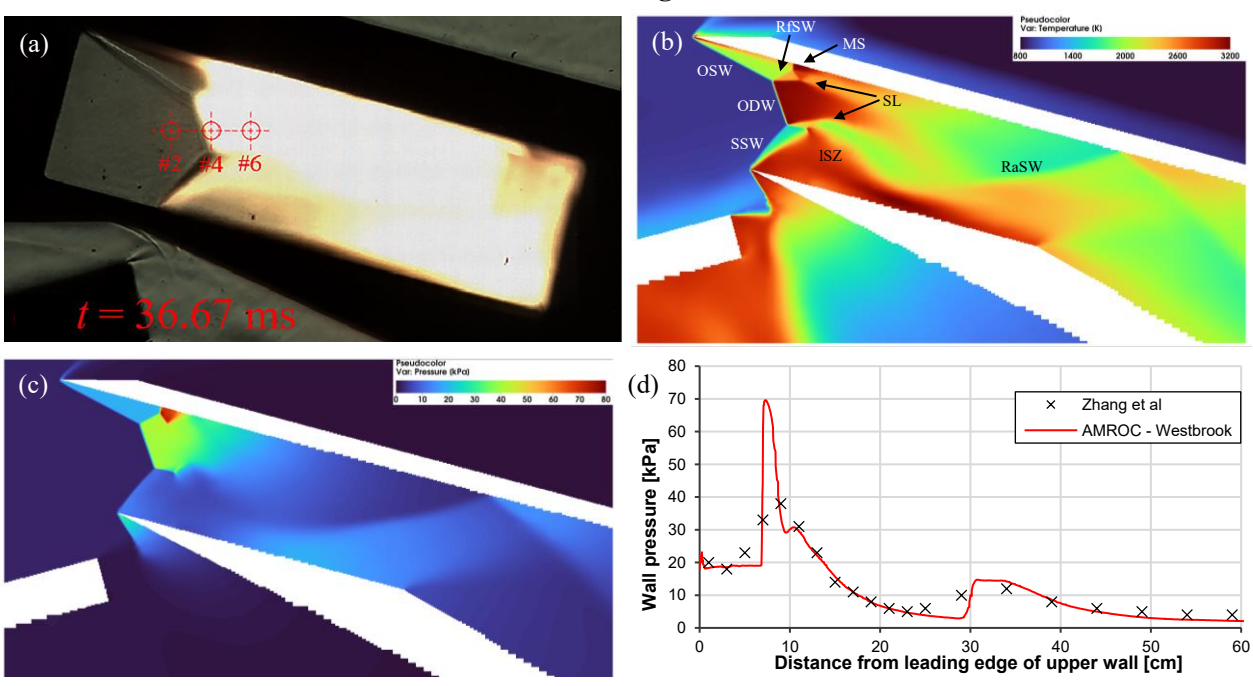


Fig. 9 Comparison of numerical simulation and LAS experiment: (a) schlieren image, (b) temperature, (c) pressure, (d) pressure distribution on upper wall.

In Fig. 9(a - c) the experiment schlieren image is compared with the numerical flow field from our CFD simulation using the Westbrook mechanism. The shockwave and detonation wave structures are well resolved, with the same structure as the strong case discussed in Section VI. Additionally, the measured β_w of 84° agrees with the simulation result of 86.5° and the measured L_w of 28 mm matches our simulation ($L_w = 30$ mm). From Fig. 9(d), the pressure distribution over the upper wall shows good agreement between numerical and experimental results. The large pressure peak is caused by the Mach stem attached to the wall and the RfSW. The SSW is shorter in the experiment, as the detonation front forms slightly closer to the lower wall of the combustor. It is possible that the bluntness of the upper lip of the combustor increases the width of the OSW, moving the ODW front to a lower position.

The minimum cell requirements, CPU time and required time steps for this simulation are similar to the strong case, and adaptive mesh refinement is equally effective. This second experiment provides an additional test case for validation of numerical methods and has been recreated correctly using AMROC.

IX. Influence of Reaction Mechanisms and Resolution

Further simulations were performed to assess the accuracy of the numerical predictions. For the strong case, simulations were conducted with three refinement levels, corresponding to half the resolution of the original simulation. In these simulations, the minimum cell dimensions are $1.26 \text{ mm} \times 0.73 \text{ mm}$. Simulations were conducted using both reaction mechanisms, with the results documented in Fig. 10. It was found that at lower resolution, there is slight divergence from the flow field presented in Section VI. For both cases, L_w decreases by 25%, and the MS becomes poorly resolved. This observation is not unexpected since the reaction behind the shock front is very sensitive to the resolution across the induction zone. In addition, coarser boundaries have a detrimental effect on accuracy, as in the used Cartesian embedded boundary method the inlet geometry tips appear blunter which causes some premature reaction at the combustor leading edge.

Comparing the temperature and pressure distributions, the shockwave structure is largely mechanism independent for the strong case. The Jachimowski mechanism predicted enhanced reaction at wall boundaries, which caused greater mesh refinement in these areas. In Fig. 10(b), some distortion of the MS is observed, but there is insufficient resolution to resolve the shockwave - boundary layer interaction.

By contrast, the weak case is much more sensitive because deflagrative combustion occurs across the entire shock front, requiring accurate representation of varying induction lengths. The Jachimowski mechanism was found to be more suitable for simulations of the weak case.

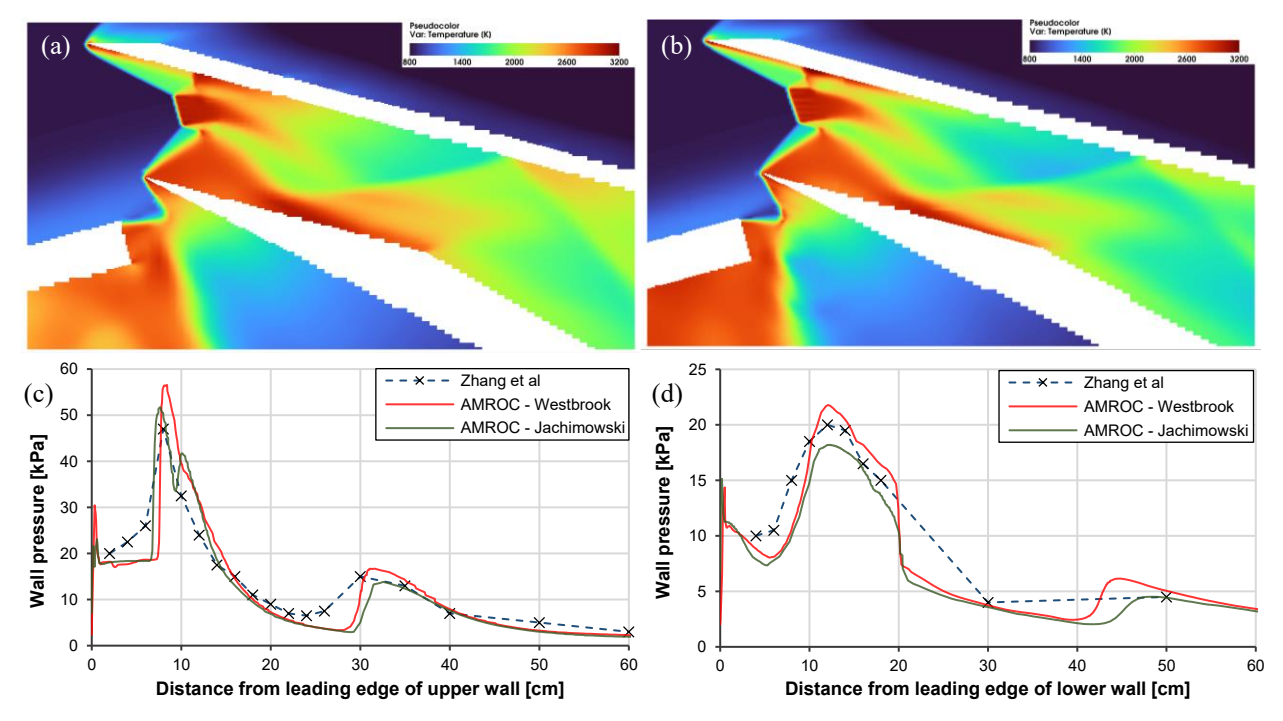


Fig. 10 Comparison of reaction mechanisms for strong ODW: (a) Westbrook, (b) Jachimowski, (c) pressure distribution on upper wall, (d) pressure distribution on lower wall.

X. Conclusion

This paper reports the successful CFD validation of three external injection ODWE experiments using AMROC. The provided geometry, numerical setup, and detailed inflow parameters make these configurations now easily accessible and provides a set of fully reproducible ODWE benchmarks for other simulation codes. While the authors of the experiments have published CFD results for the strong ODW configuration, we report the first simulations of the weak ODW case. Simulating the full ODWE in one computation offers several advantages including reduced computational costs and allows investigation of interaction effects between the inlet ramp and combustor entrance.

For the strong and LAS cases, the simulations successfully replicate the detailed flow structures observed in the experiment. Predicted detonation wave angles, detonation front lengths and pressure distributions are matched by the experiment. In addition, post detonation pressure and temperature are provided, and predicted induction lengths in the OSW and SSW are reported. We have provided the minimum cell resolutions which allowed accurate calculations of the flow field, along with CPU time estimates and required time steps.

Results for the weak case with ideal inflow conditions show deflagrative combustion across most of the shock front. The OSW angle and temperature, pressure and H₂O distributions of the flow field are provided as another benchmark for numerical methods. From the analysis of boundary layer effects on the inlet ramp, we have demonstrated that a reactive boundary layer increases the ODW length. Therefore, it is likely that a disturbance preceding the combustor is necessary to increase the detonation front length to match what is observed in the schlieren image. While the authors report that the shock front and flame in the combustor remained stabilized during the test, further images of the startup sequence are not provided which could be valuable in this investigation. In summary, the weak case is a very demanding configuration to reproduce numerically as it is sensitive to the reaction mechanism and requires a model that replicates induction lengths very accurately.

Appendix

A. Geometry

Table 5 Geometry for strong ODW.

Strong ODW	x coordinate [cm]	y coordinate [cm]
	0.000	0.000
T.1.4	11.591	0.000
Inlet ramp	155.324	38.513
	154.548	41.411
	152.082	53.403
Upper combustor wall	215.834	36.322
and nozzle	220.834	36.322
	157.082	53.403
	155.898	44.461
Lower combustor wall and nozzle	244.992	-1.000
and nozzie	175.217	39.285

Table 6 Geometry for weak ODW.

Weak ODW	x coordinate [cm]	y coordinate [cm]
	2.462	2.520
In1-4	14.053	2.520
Inlet ramp	157.786	41.033
•	157.010	43.931

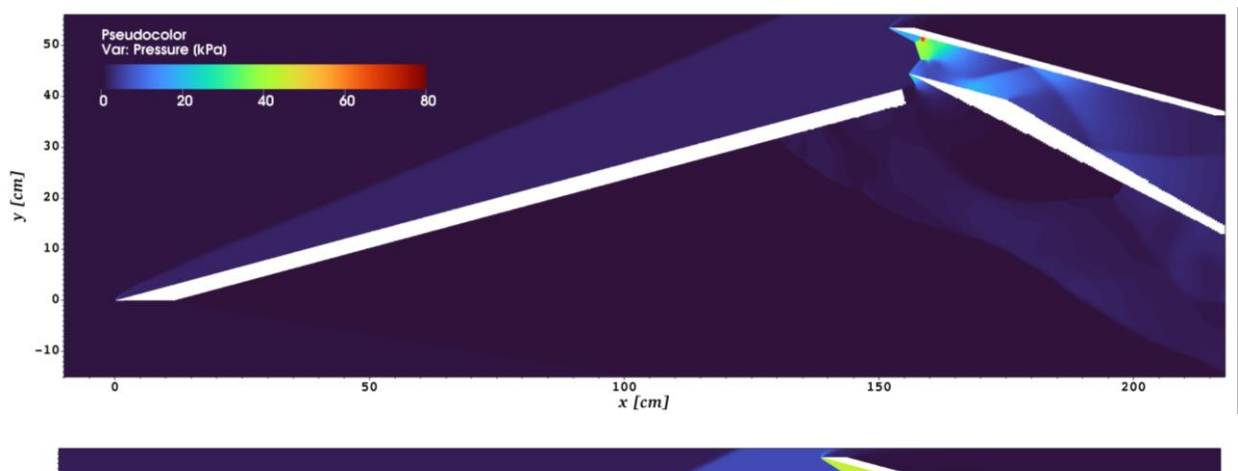
•	139.594	58.286
Upper combustor wall	217.834	37.322
and nozzle	222.834	37.322
	144.594	58.286
- 1	157.898	45.461
Lower combustor wall and nozzle	246.992	0
and nozzie	177.217	40.285

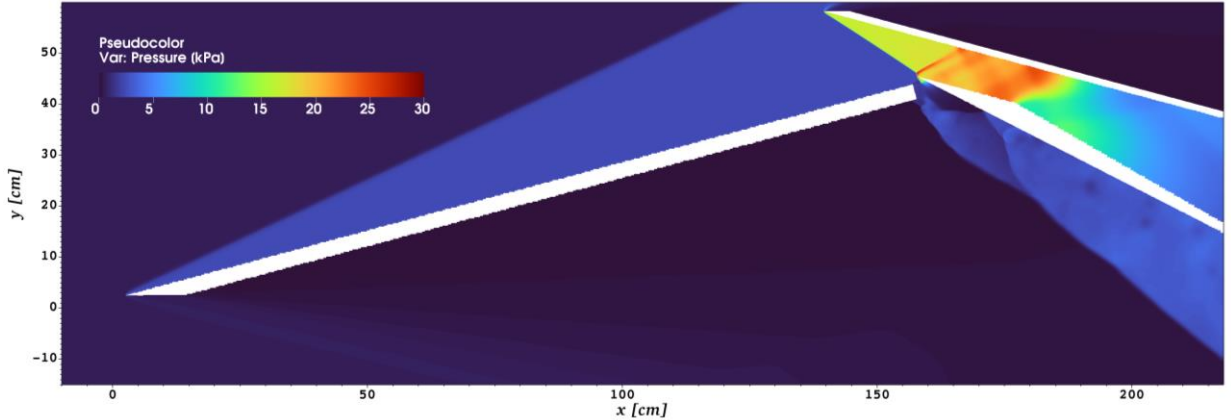
B. Numerical Setup

Table 7 Simulation parameters for strong ODW.

	•	9	
M_{∞}	6.037	$P_{s,\infty}$ [kPa]	0.332
Φ	0.460	$T_{s,\infty}$ [K]	429.9
Gas mixture [mol]	1.087	$O_2 + 1.000 H_2 + 4.037 N_2 + 0.$	052 Ar
·		<u>.</u>	
Coarse mesh size	440 x 260	Mesh levels	4
Refinement factors	2, 2, 2	Domain [cm]	228 x 76
Target CFL	0.90	Reaction Mechanism	Westbrook
	Table 8 Simulation par	rameters for weak ODW.	
M_{∞}	4.6	$P_{s,\infty}$ [kPa]	0.550
Φ	0.820	$T_{s,\infty}$ [K]	410.3
Gas mixture [mol]	0.610	$O_2 + 1.000 H_2 + 2.265 N_2 + 0.$	029 Ar
Construction	400 240	M1-11-	4
Coarse mesh size	400 x 340	Mesh levels	
Refinement factors	2, 2, 2	Domain [cm]	228 x 80
Target CFL	0.90	Reaction Mechanism	Jachimowski
Ta	ble 9 Simulation param	neters for LAS Strong Case.	
M_{∞}	5.912	$P_{s,\infty}$ [kPa]	0.355
Φ	0.465	$T_{s,\infty}$ [K]	491
Gas mixture [mol]	1.075	$O_2 + 1.000 H_2 + 3.994 N_2 + 0.$	051 Ar
Coarse mesh size	440 - 260	Mesh levels	4
-	440 x 260		
3Refinement factors	2, 2, 2	Domain [cm]	228 x 76
Target CFL	0.90	Reaction Mechanism	Westbrook

C. Full Domain for Strong and Weak Case





References

- [1] Z. Zhang, C. Wen, C. Yuan, Y. Liu, G. Han, C. Wang and Z. Jiang, "An Experimental Study of Formation of Stabilized Oblique Detonation Waves in a Combustor," *Combustion and Flame*, (Article) 111868, vol. 237, 2022.
- [2] Z. Zhang, K. Ma, W. Zhang, X. Han, Y. Liu and Z. Jiang, "Numerical investigation of a Mach 9 oblique detonation engine with fuel pre-injection," *Aerospace Science and Technology*, (Article) 106054, vol. 105, 2020.
- [3] R. Deiterding, "Parallel Adaptive Simulation of Multi-dimensional Detonation Structures PhD dissertation," Brandenburg Technical University, Cottbus, Germany, 2003.
- [4] R. Deiterding, "A parallel adaptive method for simulating shock-induced combustion with detailed chemical kinetics in complex domains," *Computers and Structures*, vol. 87, pp. 769-783, 2009.
- [5] R. J. Kee, F. M. Rupley, E. Meeks and J. A. Miller, "CHEMKIN-III: A FORTRAN Chemical Kinetics Package for the Analysis of Gas-phase Chemical and Plasma Kinetics," Sandia National Laboratories, Albuquerque, New Mexico, 1996.
- [6] C. K. Westbrook, "Chemical kinetics of hydrocarbon oxidation in gaseous detonations," *Combustion and Flame*, vol. 46, pp. 191-210, 1982.
- [7] C. J. Jachimowski, "An Analytical Study of the Hydrogen-Air Reaction Mechanism With Application to Scramjet Combustion," NASA, Hampton, Virginia, 1988.
- [8] P. Kaps and P. Rentrop, "Generalized Runge-Kutta methods of order four with stepsize control for stiff ordinary differential equations," *Numerische Mathematik*, vol. 33, pp. 55-68, 1979.
- [9] M. J. Berger and P. Colella, ""Local adaptive mesh refinement for shock hydrodynamics," *Journal of Computational Physics*, vol. 82, no. 1, pp. 64-84, 1989.
- [10] R. Deiterding, "Block-structured Adaptive Mesh Refinement Theory, Implementation and Application," *ESAIM: Proceedings*, vol. 34, pp. 97-150, 2011.

- [11] R. Deiterding, "High-Resolution Numerical Simulation and Analysis of Mach Reflection Structures in Detonation Waves in Low-Pressure H2-O2-Ar mixtures: A summary of Results Obtained with the Adaptive Mesh Refinement Framework AMROC," *Journal of Combustion*, vol. Volume 2011, p. Article ID 738969, 2011.
- [12] X. Cai, J. Liang, R. Deiterding, Y. Mahmoudi and M. Sun, "Experimental and numerical investigations on propagating modes of detonations: Detonation wave/boundary layer interaction," *Combustion and Flame*, vol. 190, pp. 201-215, 2018.
- [13] H. Peng, Y. Huang, R. Deiterding, Z. Luan, F. Xing and Y. You, "Effects of jet in crossflow on flame acceleration and deflagration to detonation transition in methane—oxygen mixture," *Combustion and Flame*, vol. 198, pp. 69-80, 2018.
- [14] H. Wei, X. Zhang, H. Zeng, R. Deiterding, J. Pan and L. Zhou, "Mechanism of end-gas autoignition induced by flame-pressure interactions in confined space," *Physics of Fluids*, vol. 31, 2019.
- [15] W. Zhang, Z. Zhang, X. Han, C. Yuan, Y. Liu, L. Ma and W. Ren, "On the determination of the standing oblique detonation wave in an engine combustor using laser absorption spectroscopy of hydroxyl radical," *Aerospace Science and Technology*, (Article) 109344, vol. 152, 2024.
- [16] X. Han, Y. Liu, Z. Zhang, W. Zhang, C. Yuan, G. Han and Z. Jiang, "Experimental demonstration of forced initiation of kerosene oblique detonation by an on-wedge trip in an ODE model," *Combustion and Flame*, vol. 258, 2023.
- [17] P. Zhang, Y. Wang and Y. Wang, "Development of pulse-type skin friction balance use in shock tunnel," *Review of Scientific Instruments*, vol. 96, no. 4, 2025.
- [18] The Engineering ToolBox, "Heat Capacity," (2005). [Online]. Available: https://www.engineeringtoolbox.com/heat-capacity-d 338.html. [Accessed 12 04 2024].